Role of aluminum in aggregated TiO_2 spheres for photocatalytic degradation of RBR X-3B

PING ZHAO, YINGHAO DONG, HONGLIANG XIN, WENJIE ZHANG*
School of Environmental and Chemical Engineering, Shenyang Ligong University, Shenyang 110159, China

Aggregated Al-TiO_2 spheres were synthesized by sol-gel method using graphite sphere template. The diameter of the spheres is almost as large as 500 nm. Anatase TiO_2 forms in all the samples, and doping of aluminum in the anatase TiO_2 skeleton hinders crystal growing. The binding energies of Ti2$p_{3/2}$ and Ti2$p_{1/2}$ electrons decrease after doping aluminum in TiO_2 spheres. The surface area of the aggregated Al-TiO_2 spheres is doubled after doping 0.1% of aluminum in the TiO_2 skeleton. The maximum photocatalytic degradation efficiency is obtained by the 0.1%Al-TiO_2 aggregated spheres. Decoloration efficiency on the 0.1%Al-TiO_2 aggregated spheres decreases slowly after several treating cycles.

(Received October 14, 2018; accepted August 20, 2019)

Keywords: Photocatalytic, Sol-gel, TiO_2, Doping, Aluminum

1. Introduction

Organic pollutants in wastewater can be removed through photocatalytic oxidation [1-3]. The large scale application of this technique in wastewater treating plant is very interesting. Illumination and photocatalytic material are the two major components in this technique, while photocatalyst is the most important factor in influencing wastewater removal efficiency [4-6]. TiO_2 is the most studied material since it seems to have the greatest activity among various kinds of materials. TiO_2-based materials can be utilized in almost all the fields relating to photocatalytic technique [7,8].

Modification of TiO_2-based material is an effective way to improve its activity [9,10]. For example, metal ions can be doped into TiO_2 crystalline skeleton through different methods [11-14]. Ion doping in TiO_2 can retard recombination of photogenerated electron-hole pairs [15,16]. Either the formation of lower conduction band level or the introduction of electron trap in TiO_2 is capable of promoting quantum efficiency and absorption of illumination at longer wavelength. The charge carriers' lifetime can be extended, and therefore photocatalytic activity is enhanced.

Porous photocatalytic materials are used to promote photocatalytic activity and to improve the efficiency of photo-electron-conversion, because large surface area and porous structure are usually beneficial to strong adsorption ability. Many microporous and mesoporous photocatalytic materials have been prepared accordingly, such as TiO_2 [17], Nb_2O_5 [18], ZnO-SnO_2 [19] and titanates [20,21].

In the present work, aluminum doped TiO_2 in an aggregated sphere form was synthesized by sol-gel method using a mixed precursor of aluminum isopropoxide and tetrabutyl titanate. The graphite sphere template was prepared through a hydrothermal route. The effects of aluminum doping concentration on the physiochemical properties and photocatalytic activity of the materials were investigated. The materials were characterized by X-ray diffraction, scanning electron microscopy, X-ray photoelectron spectroscopy, and surface area and pore analyses. Adsorption and photocatalytic degradation of Reactive Brilliant Red X-3B (RBR X-3B) dye on the materials were studied.

2. Experimental methods

2.1. Synthesis of Al-TiO_2 aggregated spheres

Al-TiO_2 aggregated spheres were prepared by a sol-gel method. Firstly, the graphite spheres were synthesized through a hydrothermal route [22]. 50 mL of 1 mol/L glucose was put into a PTFE container. The container was maintained in a stainless steel reactor at 180 ^oC for 12 h. After cooling, the suspension in the container was centrifuged and filtrated. The solid product was cleaned using distilled water and ethanol, and then the material was dried at 80 ^oC for 4 h to obtain the graphite spheres.

Tetrabutyl titanate and aluminum isopropoxide were used as the titanium and aluminum source. A certain amount of aluminum isopropoxide and 1 mL tetrabutyl titanate were dissolved in 10 mL anhydrous ethanol to prepare solution A. The graphite spheres were mixed with 10 mL anhydrous ethanol, and the mixture was stirred in a beaker for 10 min to obtain suspension B. Solution A was dropped into suspension B under stirring and the mixture was treated in an ultrasonic cleaner for 60 min. After staying at room temperature for 24 h, the suspension was

filtrated and cleaned using distilled water and ethanol. The solid was dried at 80 °C for 6 h, followed by 2 h of calcination at 600 °C. The obtained materials were ground and marked as *x*%Al-TiO_2 [*x*%= *n*(Al)/*n*(Ti) ×100%].

2.2. Characterization methods

Crystal structure of the materials were analyzed by D8 Advance X-ray diffractometer at 40 kV and 40 mA for monochromatized Cu Kα (λ=1.5416Å) radiation. Surface morphologies of the materials were measured on QUANTA 250 scanning electron microscope (HV 25kV). Chemical environment of element was analyzed by ESCALAB 250Xi X-ray photoelectron spectroscopy (Al *K*α, pass energy 100.0 eV, energy step 1.000 eV). The binding energies were referenced to the C1s peak at 284.8 eV of the surface adventitious carbon. Specific surface area and porous structure measurements were performed using a surface area and pore size analyzer (F-sorb 3400).

2.3. Decoloration of RBR X-3B

Adsorption and photocatalytic decolorization of RBR X-3B were examined in a lab scale reactor. 10 mg photocatalyst and 50 mL of 40 mg/L RBR X-3B solution were mixed in a 100 mL quartz beaker in the dark. Adsorption-desorption equilibrium of the dye on the material was reached after stirring for 30 min. A 20 W UV-light lamp was used as the light source. The irradiation intensity at λ=253.7 nm was 1200 μW/cm^2, as measured by an actinometer. Photocatalytic degradation of RBR X-3B solution was conducted for 30 min during stirring. Absorbance of the solution was measured by a 721E spectrophotometer at the maximum absorption wavelength of 539 nm. Lambert-Beer theory was used to calculate the concentration of RBR-X3B solution.

3. Results and discussion

XRD patterns of Al-TiO_2 aggregated spheres with different Al doping concentration are shown in Fig. 1. According to the pattern in JCPDF (21-1272), all the diffraction peaks can be identified as anatase TiO_2. Although aluminum doping concentration varies from 0.1% to as high as 5% in the samples, there is no diffraction peak of aluminum oxide in the patterns. The most preferred orientation is the (101) plane, which is the same for all the samples with different aluminum doping concentration. Crystallite size of the anatase TiO_2 crystal is calculated based on the intensity of the (101) plane using Scherrer formula. The pure TiO_2 spheres have a crystallite size of 30.3 nm. On the other hand, the crystallite sizes are 25.4, 24.6 and 23.8 nm for the aggregated spheres containing 0.1%, 1% and 5% aluminum. Doping of aluminum in the anatase TiO_2 skeleton hinders crystal growth.

Lattice parameters of anatase TiO_2 in Al-TiO_2 aggregated spheres are given in Table 1. The prepared anatase TiO_2 is in the tetragonal system. The TiO_2 crystal cell expands at *a* and *b* direction, but shrinks at *c* direction with increasing Al concentration. The doping of aluminum causes a noticeable distortion of the anatase TiO_2 cell, leading to a continuous expansion of the cell volume with increasing aluminum doping concentration. The radius of Al^{3+} ion is 53.5 pm, while the radius of Ti^{4+} ion is 60.5 pm. Ti^{4+} in the anatase TiO_2 skeleton cannot be substituted by the doped Al^{3+} ion, because if in that case, the cell volume will decrease instead of expanding after doping. Therefore, the doped Al^{3+} ions must enter into the octahedral void or tetrahedral void in the anatase TiO_2 lattice.

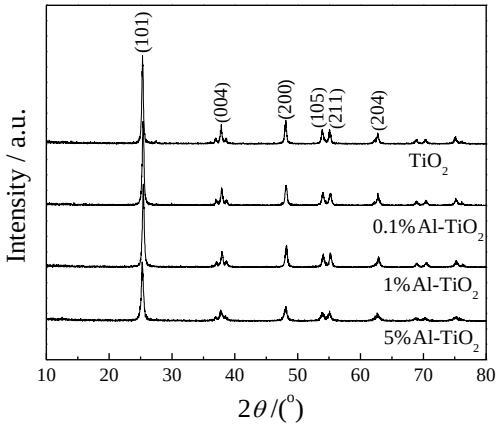

Fig. 1. XRD patterns *of Al-TiO_2 aggregated spheres with different Al doping concentration*

Table 1. Lattice parameters of anatase TiO_2 in Al-TiO_2 aggregated spheres

Sample	*a*(=*b*) /nm	*c* /nm	*V* /nm^3
TiO_2	0.37717	0.95140	0.13534
0.1%Al-TiO_2	0.37743	0.95128	0.13551
1%Al-TiO_2	0.37744	0.95079	0.13575
5%Al-TiO_2	0.37860	0.95025	0.13621

Fig. 2 presents SEM images of Al-TiO_2 aggregated spheres with respect to aluminum concentration. As can be seen from the figure, all the samples are composed of aggregated spheres that are hardly be affected by the variation of aluminum doping content. The diameter of the spheres is almost as large as 500 nm. The graphite spheres were used as template to prepare the Al-TiO_2 aggregated spheres. The graphite spheres were burnt out during calcination to leave holes in the Al-TiO_2 aggregated spheres. At the same time, dehydration of titanium-hydroxyl groups during so-gel process can lead to slight aggregation of the obtained Al-TiO_2 spheres. The doping of aluminum has little effect on the formation of Al-TiO_2 spheres.

Fig. 3 gives N_2 desorption isotherms of Al-TiO_2 aggregated spheres. The adsorbed volume of N_2 increases with rising aluminum doping concentration. The isotherms show a typical porous structure in the materials. N_2 molecules may be adsorbed on the surface of the samples

in mono or multilayer at low N_2 relative pressure. Capillary condensation happens at high relative pressure. A sharp increase of the adsorbed N_2 volume occurs at N_2 relative pressure higher than 0.8. The abrupt increase of adsorbed volume is related to the macropores in the materials.

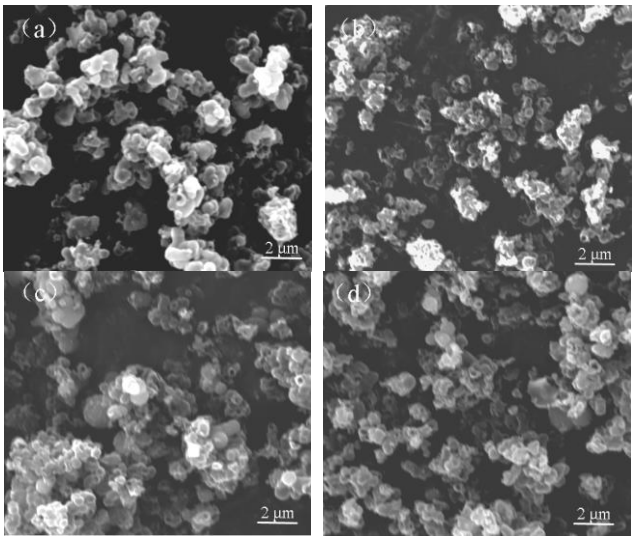

Fig. 2. SEM images of Al-TiO_2 aggregated spheres as a factor of Al concentration.(a) TiO_2, (b) 0.1%Al-TiO_2, (c) 1%Al-TiO_2, (d) 5%Al-TiO_2

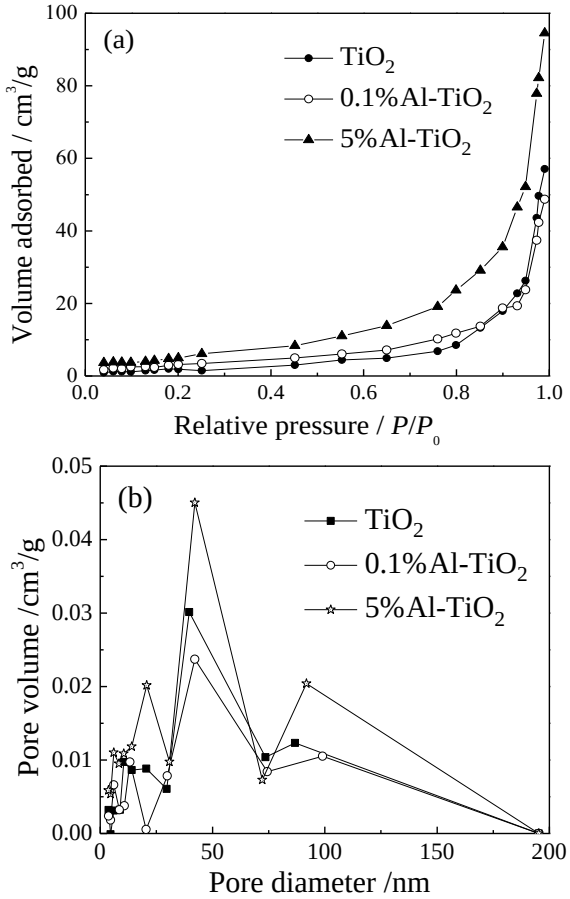

Fig. 3. (a) N_2 desorption isotherms and (b) BJH pore size distribution of Al-TiO_2 aggregated spheres

Table 2 gives BET surface area, average pore size and total pore volume of the Al-TiO_2 aggregated spheres. The as-prepared pure TiO_2 spheres have a very small BET surface area of 5.9 m^2/g. The surface area is doubled after doping 0.1% of aluminum in the TiO_2 skeleton. It is interesting that doping of aluminum may cause an apparent enlargement in the specific surface area. This might be due to the restrained crystal growth of TiO_2 crystal after doping of aluminum. The doping of aluminum also causes shrinking pore size and enlarging pore volume. The average pore size of the doped TiO_2 spheres is in mesoporous range.

Table 2. BET surface area and porous properties of Al-TiO_2 aggregated spheres

Sample	BET surface area / m^2/g	Average pore size /nm	Pore volume /cm^3/g
TiO_2	5.9	64.9	0.0848
0.1%Al-TiO_2	11.9	28.4	0.0961
1%Al-TiO_2	13.0	34.2	0.1120
5%Al-TiO_2	19.7	38.0	0.1582

Fig. 4 shows XPS O1*s* and Ti2*p* spectra of TiO_2 and 0.1%Al-TiO_2 aggregated spheres. The spectrum of O1*s* electrons in the materials can be divided into two binding energy peaks situating at 529.3 and 531.5 eV. The first peak is due to O^{2-} state [23], and the second peak is related to oxygen in Ti-OH. The binding energies of the two states of oxygen do not change after doping of aluminum. The binding energy peaks at 463.5 and 457.8 eV in Fig. 4b correspond to Ti2$p_{3/2}$ and Ti2$p_{1/2}$ electrons in the materials. It can be ascertained that titanium is in the Ti^{4+} oxidation state [24]. The binding energies decease after doping aluminum in TiO_2 spheres, so that electron transition from aluminum to titanium must occur in the doped material.

Fig. 5 shows decoloration of RBR X-3B dye on the mesoporous Al-TiO_2. The dye can be removed from the solution by adsorption and photocatalytic degradation pathways. The total amount of RBR X-3B molecules that are adsorbed on the surface of the materials reaches the maximum value after adsorption-desorption equilibrium. However, the materials can only remove a very small percent of the dye by adsorption. The subsequent photocatalytic degradation process is the major pathway for removal of the dye. Photocatalytic degradation efficiency depends on the activity of the photocatalyst. Nearly 33% of the initial dye molecules are degraded on the pure TiO_2 spheres after 30 min of irradiation. Photocatalytic activity of the doped Al-TiO_2 spheres depends on aluminum concentration. A suitable concentration of aluminum in the Al-TiO_2 spheres can apparently enhance the activity of the material. The optimal Al doping concentration is 0.1% when the maximum photocatalytic degradation efficiency occurs on

the 0.1%Al-TiO_2 aggregated spheres. 44.9% of the dye is degraded on 0.1%Al-TiO_2 aggregated spheres after 30 min of reaction. Normally, photocatalytic degradation of organic substance obeys the law of first order reaction. The apparent reaction rate constants are 0.019 and 0.031 min^{-1} on pure TiO_2 and the 0.1%Al-TiO_2 aggregated spheres, respectively.

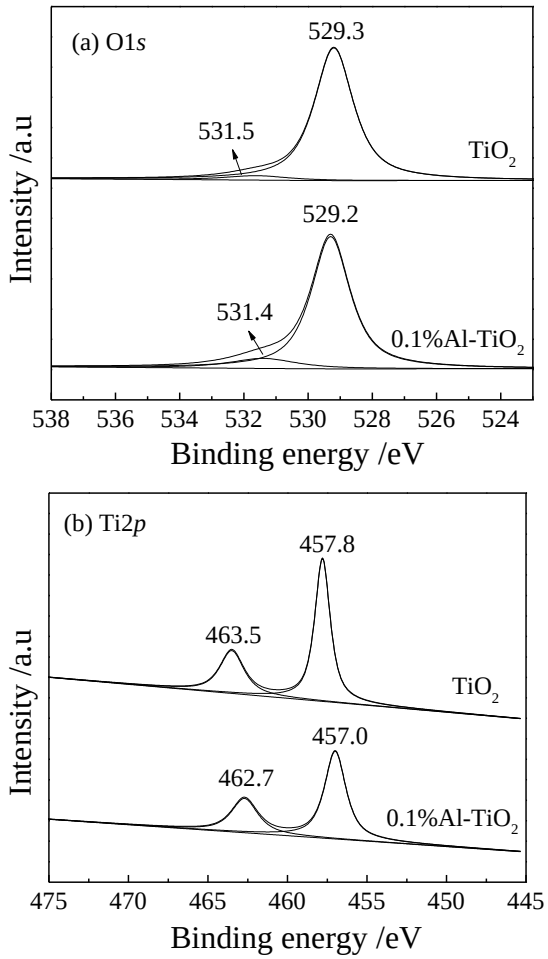

Fig. 4. XPS spectra of TiO_2 and 0.1%Al-TiO_2 aggregated spheres

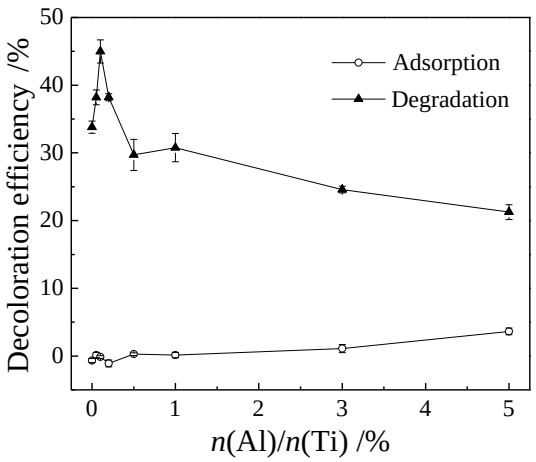

Fig. 5 Decoloration of RBR X-3B on Al-TiO_2 aggregated spheres with respect to Al doping concentration

The reusability of TiO_2 and 0.1%Al-TiO_2 aggregated spheres for photocatalytic degradation of RBR X-3B is compared in Fig. 6. The photocatalyst was filtrated after decoloration process. The obtained powders were washed with distilled water and dried in the furnace at 80 ^oC for 5 h. Each decoloration cycle includes adsorption-desorption equilibrium and photocatalytic process. The reaction system was illuminated for 75 min in each cycle. Both of the decoloration efficiencies on the pure TiO_2 and 0.1%Al-TiO_2 aggregated spheres slightly decrease after more cycles. This is due to the loss of fine particles during filtration of the powders. As can be seen in the figure, decoloration efficiency on the 0.1%Al-TiO_2 aggregated spheres decreases from nearly 100% in the first cycle to 80% in the fifth cycle. At the same time, decoloration efficiency on the pure TiO_2 spheres decreases from 60.2% in the first cycle to 41.5% in the fifth cycle.

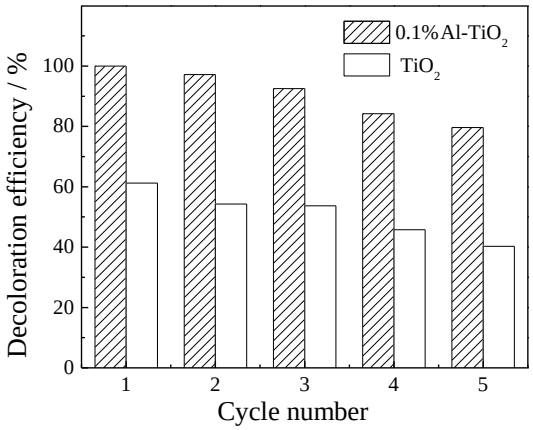

Fig. 6. Reusability of TiO_2 and 0.1%Al-TiO_2 spheres for photocatalytic degradation of RBR X-3B

4. Conclusions

Aluminum doping can influence the properties of Al-TiO_2 aggregated spheres. All the samples are composed of anatase TiO_2 with the preferred orientation in the (101) plane. The electron binding energies in the Ti^{4+} oxidation state decrease after doping aluminum, as well as an apparent enlargement in the specific surface area. The apparent reaction rate constants are 0.019 and 0.031 min^{-1} on pure TiO_2 and the 0.1%Al-TiO_2 aggregated spheres, respectively. Decoloration efficiency on the 0.1%Al-TiO_2 aggregated spheres decreases from nearly 100% in the first cycle to 80% in the fifth cycle.

Acknowledgments

This work was supported by Scientific Research Project of Liaoning Provincial Education Department (No. LG201913).

References

[1] A. Fujishima, T. N. Rao, D. A. Tryk, J. Photochem. Photobio. C **1**(1), 1 (2000).

[2] W. J. Zhang, Y. J. Tao, C. G. Li, Mater. Res. Bull. **105**, 55 (2018).

[3] D. Chatterjee, S. Dasgupta, J. Photoch. Photobio. C **6**(2-3), 186 (2005).

[4] W. J. Zhang, Y. J. Tao, C. G. Li, J. Photoch. Photobio. A: Chem. **364**, 787 (2018).

[5] P. Zhou, J. H. Wu, W. L. Yu, G. H. Zhao, G. J. Fang, S. W. Cao, Appl. Surf. Sci. **319**, 167 (2014).

[6] W. J. Zhang, H. L. Li, Z. Ma, H. Li, H. Wang, Solid State Sci. **87**, 58 (2019).

[7] M. Bellardita, A. D. Paola, B. Megna, L. Palmisano, Appl. Catal. B: Environ. **201**, 150 (2017).

[8] W. J. Zhang, Y. X. Liu, C. G. Li, J. Phys. Chem. Solids **118**, 144 (2018).

[9] J. B. Cai, X. Q. Wu, S. X. Li, F. Y. Zheng, Appl. Catal. B: Environ. **201**, 12 (2017).

[10] W. K. Jo, S. Kumar, M. A. Isaacs, A. F. Lee, S. Karthikeyan, Appl. Catal. B: Environ. **201**, 159 (2017).

[11] W. Zhang, Y. Liu, X. Pei, X. Chen, J. Phys. Chem. Solids **104**, 45 (2017).

[12] J. Du, X. Y. Li, K. Li, X. Gu, W. Q. Qi, K. Zhang, J. Alloys Compd. **687**, 893 (2016).

[13] A. Juma, I. O. Acik, A. T. Oluwabi, A. Mere, V. Mikli, M. Danilson, M. Krunks, Appl. Surf. Sci. **387**, 539 (2016).

[14] W. J. Zhang, X. B. Pei, B. Yang, H. B. He, J. Adv. Oxid. Technol. **17**, 66 (2014).

[15] E. B. Simsek, Appl. Catal. B: Environ. **200**, 309 (2017).

[16] C. Han, J. Andersen, V. Likodimos, P. Falaras, J. Linkugel, D. D. Dionysiou, Catal. Today **224**, 132 (2014).

[17] W. Zhang, F. Bi, Y. Yu, H. He, J. Mole. Catal. A: Chem. **372**, 6 (2013).

[18] X. Y. Chen, T. Yu, X. X. Fan, H. T. Zhang, Z. S. Li, J. H. Ye, Z. G. Zou, Appl. Surf. Sci. **253**, 8500 (2007).

[19] Z. J. Wang, Z. Y. Li, H. G. Zhang, C. Wang, Catal. Commun. **11**, 257 (2009).

[20] W. Zhang, Y. Tao, C. Li, Solid State Sci. **78**, 16 (2018).

[21] W. J. Zhang, J. Yang, C. G. Li, Mater. Sci. Semicond. Process. **85**, 33 (2018).

[22] W. Zhang, Y. Liu, H. Xin, Curr. Nanosci. **14**, 209 (2018).

[23] J. Pouilleau, D. Devilliers, H. Groult, J. Mater. Sci. **32**, 5645 (1997).

[24] F. Chiker, J. P. Nogier, F. Launay, Appl. Catal. A **243**, 309 (2003).

*Corresponding author: wjzhang@aliyun.com